PERGAMON

International Journal of Heat and Mass Transfer 46 (2003) 823–835

International Journal of HEAT and MASS TRANSFER

www.elsevier.com/locate/ijhmt

Turbulent heat transfer and flow characteristics in a horizontal circular tube with strip-type inserts. Part I. Fluid mechanics

Shou-Shing Hsieh *, Feng-Yu Wu, Huang-Hsiu Tsai

Department of Mechanical and Electro-Mechanical Engineering, National Sun Yat-Sen University, Kaohsiung, 80424 Taiwan, ROC

Received 3 September 2001; received in revised form 19 August 2002

Abstract

This paper is the first of two papers that present the result of a study of turbulent flow and pressure drop in a horizontal tube with strip type inserts. Experimental data taken for air for a class of strip type inserts (longitudinal, LS and cross, CS inserts) used as a tube side heat transfer augmentative device for a single-phase cooling mode operation are presented. To broaden the understanding of the underlying physical phenomena responsible for the heat transfer enhancement, flow mechanisms through velocity measurements are combined with pressure drop measurements to develop friction factor correlations for $6500 \leqslant Re \leqslant 19\,500$ where Re is the Reynolds number. Friction factor increases were typically between 1.1 and 1.5 from low $Re(\cong 6500)$ to high $Re(\cong 19\,500)$ with respect to bare tubes.

1. Introduction

Single-phase heat transfer may be increased by artificially roughened surfaces and other augmentation techniques such as vortex generators and modifications to the duct cross-section and surface [1]. These augmentation techniques belong to the so-called passive means to increase the convective heat transfer coefficient on the tube side. Recently, attention has been paid to heat transfer enhancement by means of swirl strips, twisted tapes, and meshes in heat exchanger tubes. These tube inserts are believed to enhance convective heat transfer by creating one or more combinations of the following conditions, which increase the heat transfer coefficient:

1. continuously interrupting the development of the boundary layer of the fluid flow and increasing the degree of flow turbulence;
2. continuously increasing the effective heat transfer area;
3. continuously generating secondary flow.

The objective of the present study is to experimentally investigate the friction characteristics of air flowing through a horizontal circular tube with strip-type inserts. The paper addresses the flow characteristics, which are responsible for the heat transfer enhancement.

The average temperature of the air flow covered in this friction study was kept at 26 ± 0.5 °C approximately. Two different types of tube inserts including longitudinal strip (LS) and crossed-strip (CS) with three(two) aspect ratios (L/H; ratio of width to height of insert) for LS(CS) were used and shown in Fig. 1.

2. Previous work

Among the many techniques (both passive and active) investigated for augmentation of heat transfer rates inside circular tubes, a wide range of inserts have been utilized, particularly when turbulent flow is considered: the inserts studied included tapered spiral inserts,

* Corresponding author. Tel.: +886-07-525-2000x4215; fax: +886-07-525-4215.

E-mail address: sshsieh@mail.nsysu.edu.tw (S.-S. Hsieh).

0017-9310/03/$ - see front matter
PII: S0017-9310(02)00353-8

Nomenclature

A	cross-sectional area of bare tube (m^2)
AR	aspect ratio, L/H
D	tube hydraulic diameter, $4A/P$ (m)
dA	differential cross-sectional area (m^2)
f	friction factor (developing or fully developed) based on hydraulic diameter, $\left[-\Delta p/\left(\frac{1}{2}\rho V^2\right)\right](D/\ell)$
H	height of insert (m)
L	width of insert (m)
L_e	entrance length (m)
ℓ	length of the test tube (m)
P	perimeter (m)
p	pressure (Pa)
Δp	overall pressure drop along test tube (Pa)
R	radius of inner tube (m)
R^*	radius ratio of circumscribed circle of insert to test tube, $0.5(L^2+H^2)^{1/2}/R$
Re	Reynolds number based on tube hydraulic diameter, VD/v
r	distance from measured point to the center of cross-section (m)
r^+	dimensionless length, r/R
u	velocity component in x-direction (m/s)
u'	velocity fluctuation (m/s)
u^*	friction velocity (m/s)
u^+	dimensionless local velocity, u/u^*
V	nominal (bulk) average velocity (m/s)
x	distance along main flow direction (m)
y	distance from the tube wall (m)
y^+	dimensionless distance from wall in a turbulent shear layer, yu^*/v

Greek symbols

β	contraction ratio
η	insert affected coefficient (momentum)
θ	the measuring angular position
v	kinematic viscosity
ρ	density

Subscripts

max	maximum
o	average

Superscript

+	dimensionless

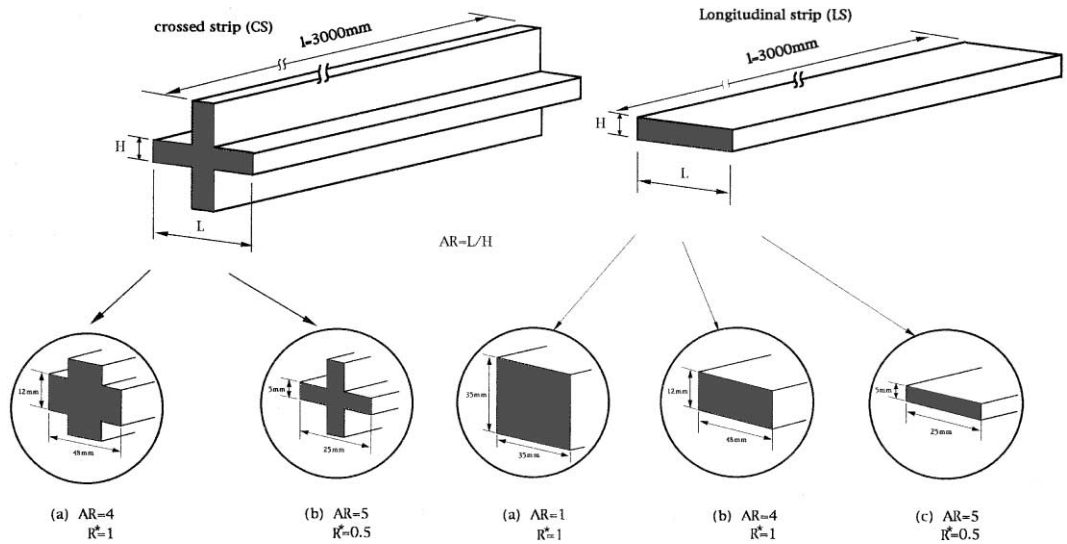

Fig. 1. Physical geometry (LS and CS) and dimensions of the inserts considered.

packing, rings, disks, streamlined shapes, mesh inserts, and spiral brush inserts [2]. Mesh or spiral brush inserts were used by Megerlin et al. [3] to enhance turbulent heat transfer in short channels subjected to high heat flux. Enhancement of up to 8.5 times in turbulent heat transfer coefficients were obtained. Maezawa and Lock [4] reported the performance of a variety of "Everter" inserts, which mix wall and core flow, and several disk inserts. Large increases in local heat transfer coefficients were observed for air flowing in an electrically heated tube; however, there was no definite improvement beyond 10 diameters downstream of the insert. Average heat transfer coefficients were doubled, but friction factors increased to as much 3.5 times. In general, these

"Everter" inserts are used in few practical turbulent flow situations for reasons of pressure drop, fouling, and structural considerations. Recently, Manglik and Bergles [5] developed thermal-hydraulic design correlations for isothermal friction factor f and Nusselt number Nu for in-tube turbulent flows with twisted-tape inserts. Experimental data were taken for water and glycerol. In addition, because the convective heat transfer coefficient is greatly increased by the centrifugal effect of swirl flow, inserts generating swirl flows are particularly attractive. Nevertheless, as one may expect, an increase in the heat transfer inevitably causes an increase in pressure drop which is generally larger than the increase of heat transfer. On the other hand, even with lower heat transfer augmentation, the insert which does not generate swirl flow may also be an eligible augmentative device, provided its net effect between the heat transfer augmentation and pressure drop increase is tolerable. Therefore, careful selection of the appropriate inserts must be made to optimize the heat transfer augmentation. As one of the practical augmentative devices, a longitudinal rectangular plate is frequently inserted in the tubes of a tubular recuperator used for waste heat recovery where the cold combustion air flowing inside the tubes is heated by the hot waste gas which flows through the tube bundle.

Previous studies have not addressed heat transfer in tubes with strip inserts through the range of turbulent flow regime and geometric combinations. The present study attempts to address these deficiencies in the literature by obtaining an understanding of flow characteristics of tubes with inserts for a wide range of geometric parameters and flow conditions.

3. Experimental setup and procedure

A stereographic view of schematic diagram of the experimental setup is shown in Fig. 2. Air at room temperature is introduced into the straight horizontal test tube. The inner diameter of test circular tube is 50 and 3000 mm in length. In all experiments, strip-type inserts were made from plexiglas, the width of which was 1 mm less than the inside diameter of the test section tube to keep no physical contact anywhere inside tube between the tube and insert. All inserts were clamped to the tube at inlet and outlet of the test section.

Air flows were measured by an orifice type flow meter ($\beta = 0.5$) with corrections applied for the temperature range covered during this study. The measured tube-side Reynolds numbers varied from 6500 to 19 500. The pressure along the test section was measured by means of a static manometer whose tubing was connected to pressure taps at each specified downstream distance. The pressure taps were perpendicular to the tube surface. For velocity and pressure drop measurements, the present studies were operated in an isothermal condition (i.e. nonheating). To verify that the isothermal conditions are reached, the temperatures at the test tube walls along the downstream and around the circumference were measured. If the variation in the measured wall temperatures was less than 1 °C, the uniformity of the

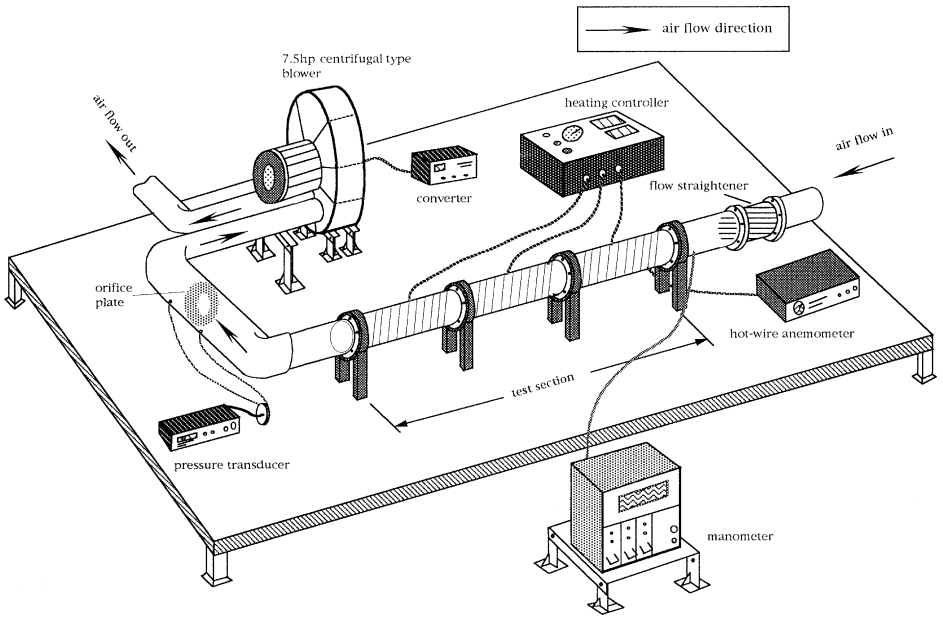

Fig. 2. Stereographic view of a schematic diagram of the experimental setup.

wall temperature distributions was considered to be satisfied.

Velocity distributions in the tube cross-section were made in streamwise, circumferential, and radial directions. Since the present experiment is for flow (i.e. nonheating) and the change of the inlet and outlet air temperature is negligible, it is demonstrated that the present flow condition can be considered as pure turbulent forced convection with negligible natural convection effect. Axial velocity uncertainty is about ±1.5% and turbulent intensity $\left(\frac{u'}{u}\right)$ uncertainty is ±4.8%.

For static pressure measurements, two static pressure tubes were placed at the center of the tube to minimize the influence on the velocity fluctuations. These static pressure measurements were used to find the friction factor f. A DISA 56C01 constant temperature hot-wire anemometer in conjunction with DISA 56N22 and 56N25 DC voltmeters was used to measure the turbulent mean flow characteristics and the velocity fluctuations. The single DISA hot-wire probe consisted of 5 mm-long prongs made of hypodermic tubing of 0.5 mm diameter; the spacing between the centers of the prongs was 1.25 mm. The stem was 30 mm long with 4 mm diameter; it tapered down to 2 mm diameter in the lower 3 mm position adjacent to the prongs. Thus, the blockage ratio of the prongs and stem in the test region was less than 4.48% (LS) and 5.36% (CS), respectively. The sensor was made from DANTEC platinum-plated tungsten wire of 5 μm diameter. As the effective length of the sensor was 1.2 mm, the aspect ratio is about 240. In view of the low wind velocities, a comparatively low overheat value of 0.65 was employed.

Room air (nonheating) was used as the working medium in the study. Air flow was obtained by a 5.52 kW electric motor driven blower on the same test stand.

In each run, data for temperatures, flow rates and pressure drops of air were recorded after steady-state conditions were reached. In fact, pressure drop tests reach steady-state instantaneously. The measurements include:

1. Temperature of the air at inlet and exit of the test section;
2. Pressure in the test section at each specified downstream position;
3. Local velocities in the test section at each specified radial, angular and downstream position;
4. Inner test tube wall temperature at several locations;
5. Five mass flow rates giving a range of Reynolds number from 6500 to 19 500.

The Darcy friction factor (f) was calculated from the pressure drop across the flow channel as

$$f = -\frac{\Delta p}{\frac{1}{2}\rho V^2}\frac{D}{\ell} \tag{1}$$

The results were compared with the friction factor for fully developed turbulent flow in smooth tube proposed by Blasius [6]. In addition to the friction factor, the entrance length was also examined and correlated in terms of the Reynolds number. Before a formal experimental run, the assessment for hydrodynamically laminar entrance length in a smooth tube was observed and compared with the existing data. Following Moffat [7], the estimated maximum uncertainties of Reynolds numbers (Re) and friction factors (f) are about 8.2% and 7.5%, respectively.

The mass flow rate (i.e. continuity equation of the velocity profile) in each case was assessed. The measured mass flow rate was calculated based on the integration of velocity distributions measured over a particular cross-section and compared with those from an orifice plate. It is found that the deviation is less than 7.5% for the worst case.

4. Results and discussion

According to the literature review, the present flow pattern is a function of following variables such as Reynolds number (Re), aspect ratio (L/H), and radius ratios (R^*) in which R^* was defined as $0.5(L^2+H^2)^{\frac{1}{2}}/R$. The R^* defined here is a blockage ratio due to the presence of the insert. Based on hydrodynamic considerations, the flow field is significantly influenced by the insert blockage and secondary flow circulation in the direction perpendicular to the flow direction. The insert increases the wetted perimeter and reduces the flow cross-sectional area.

4.1. Hydrodynamic entrance length

The hydrodynamic entrance length could be determined from Figs. 3–7 for tubes with inserts. The hydrodynamic entrance length was determined when the variation of the streamwise velocity distribution along the downstream was less than 2% (i.e., u is only a function of r) i.e., $\left[\left(\frac{u}{u_0}\right)_p - \left(\frac{u}{u_0}\right)_p - 1\right] \Big/ \left[\left(\frac{u}{u_0}\right)\right]_p \leqslant \pm 0.02$ where p stands for downstream positions for each r^+ measured. The streamwise velocity distribution at several particular cross-section along downstream distances ($x/D = 2$, 6, 12, 14, 16, 26, 34, and 54) at $Re = 6500$, 9750, 13 000, 16 250, and 19 500 for LS insert with AR = 1 is illustrated in Fig. 3. It is found that the hydrodynamic entrance length L_e/D is less than 2 due to a higher velocity ($u_0 \cong 30$ m/s at $Re = 19\,500$) and is also weakly independent of Reynolds number because even at $Re = 6500$, the u_0 can reach to about 11 m/s which is quite high compared to those of the remainder tubes. By the same token, this situation also happened for the corresponding figure for CS insert with AR = 4 with

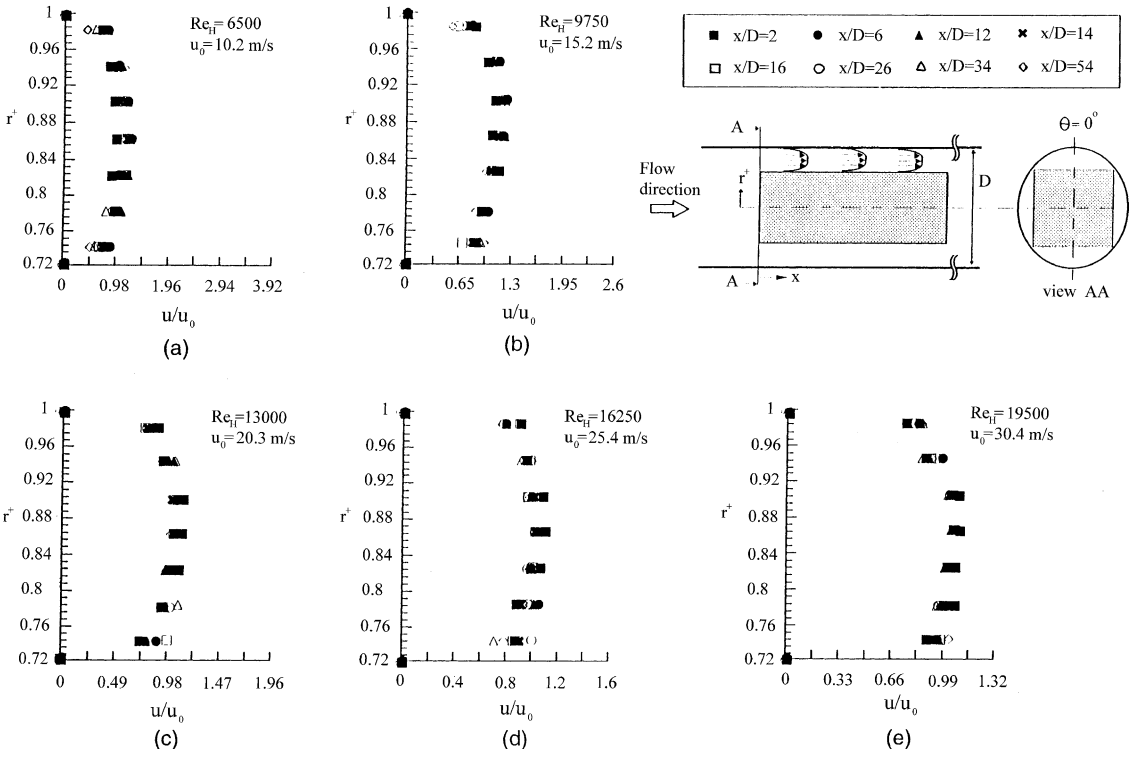

Fig. 3. Axial velocity distributions along the downstream direction for tube with LS insert and AR = 1 ($\theta = 0°$).

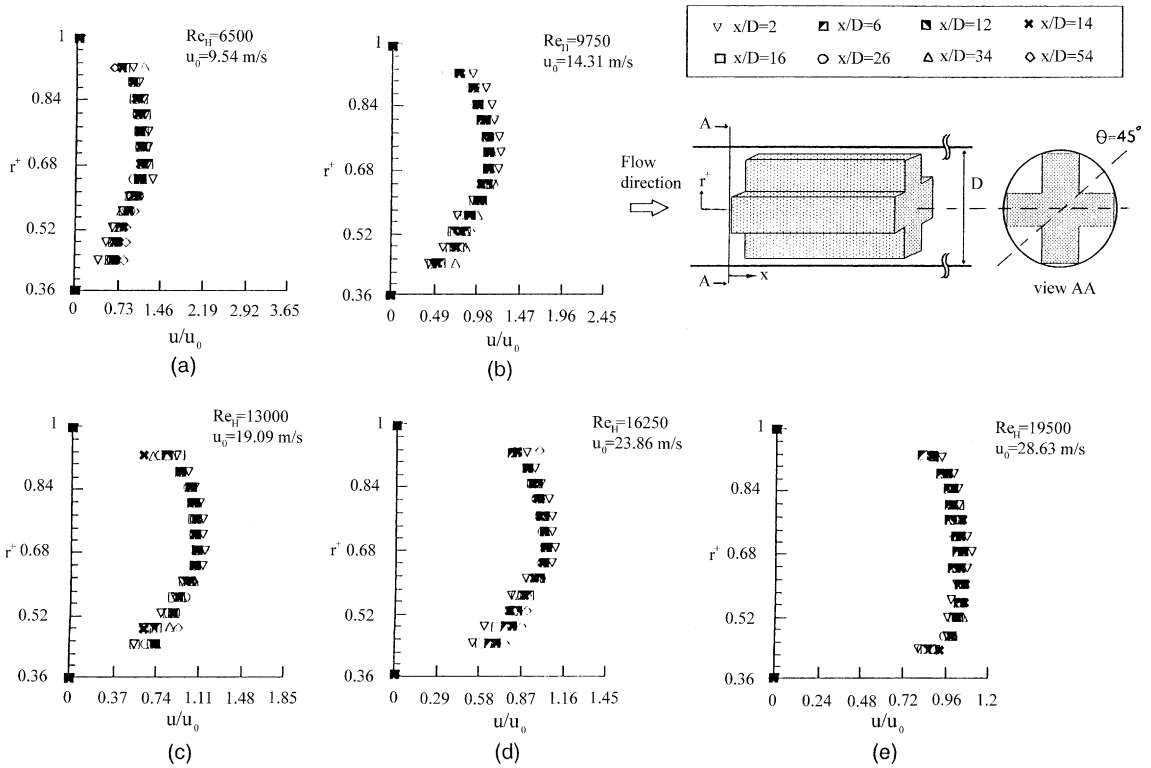

Fig. 4. Axial velocity distribution along downstream direction for tube with CS insert and AR = 4 ($\theta = 45°$).

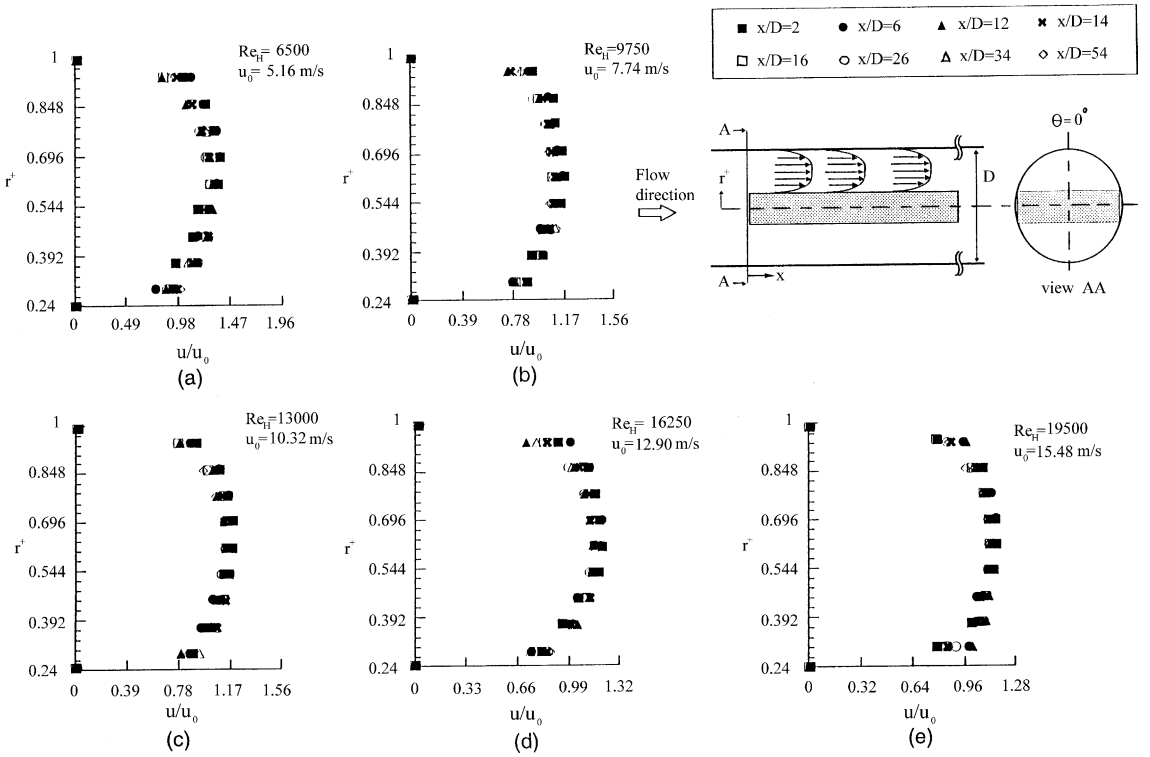

Fig. 5. Axial velocity distributions along the downstream direction for tube with LS insert and AR = 4 ($\theta = 0°$).

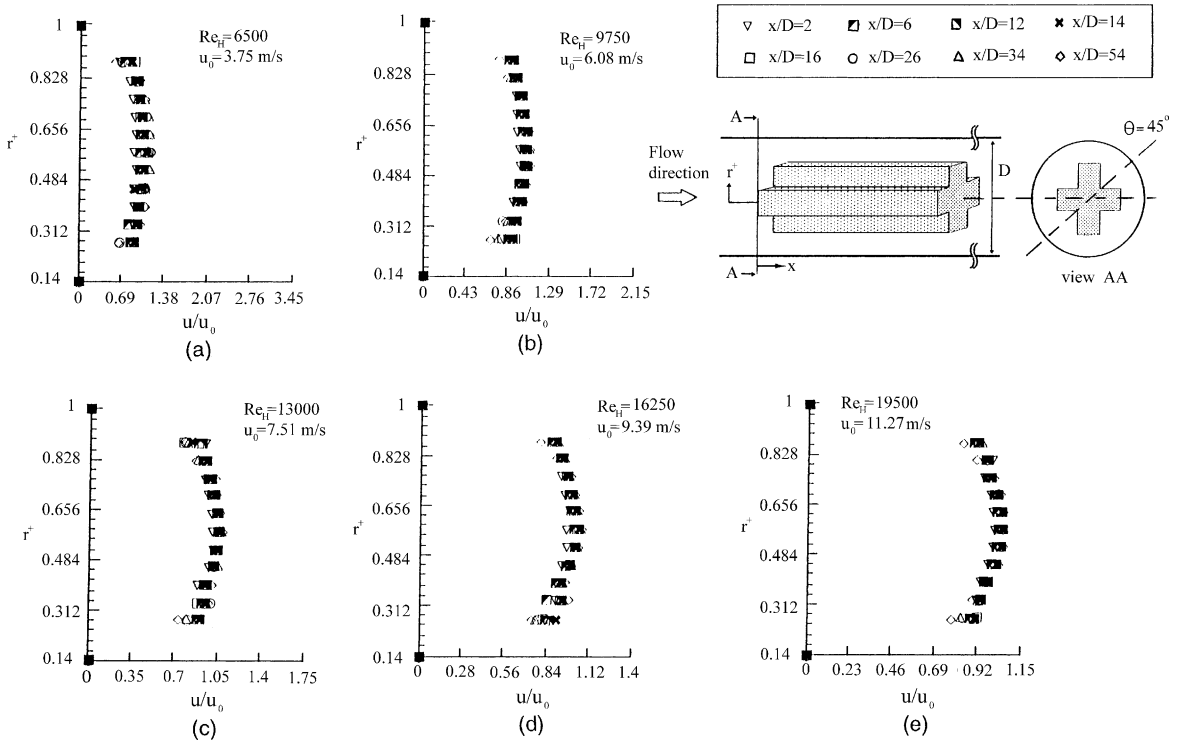

Fig. 6. Axial velocity distribution along downstream direction for tube with CS insert and AR = 5 ($\theta = 45°$).

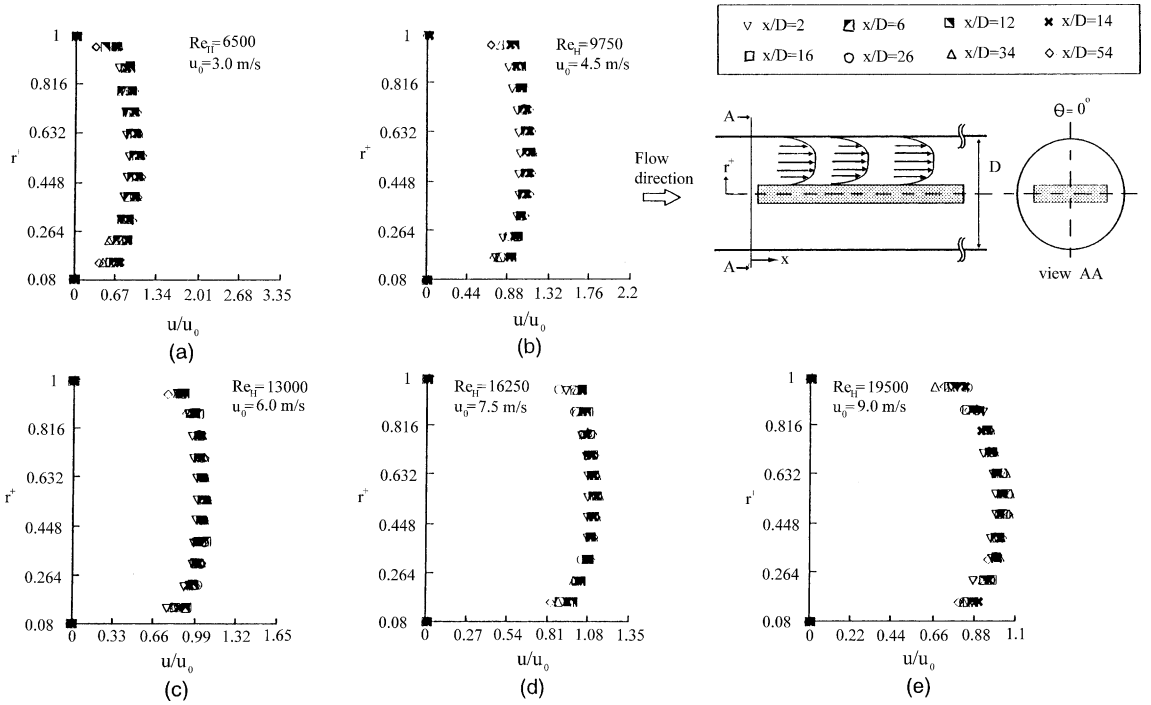

Fig. 7. Axial velocity distributions along the downstream direction for tube with LS insert and AR = 5 ($\theta = 0°$).

slight increase of L_e/D as shown in Fig. 4. And, followed by LS insert with AR = 4 in Fig. 5, CS insert with AR = 5 in Fig. 6 and LS insert with AR = 5 in Fig. 7 in which they have $x/D \approx 3$, 4 and 5, respectively. That the hydrodynamic entrance length is weakly dependent on the Reynolds number, shown in Fig. 8 as also evidenced by the previous findings. Furthermore, the entrance length dependency on *Re* is further confirmed for tubes with insert and the entrance length becomes shorter compared to the tube without insert. In addition, the

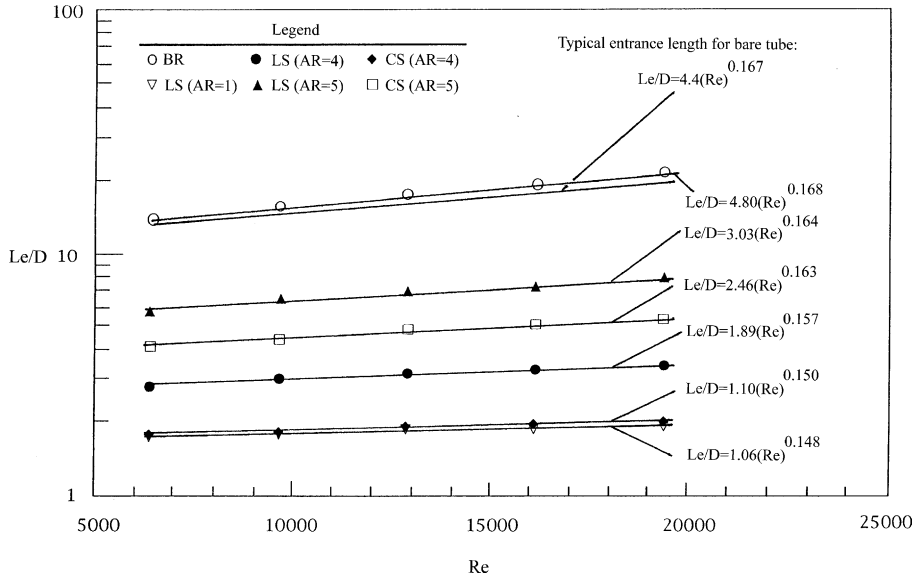

Fig. 8. The entrance length versus Reynolds number for different inserts and bare tube.

entrance length for tubes without inserts compared well with to the existing data for smooth tubes and Fig. 8. This further validates the experimental setup and the present procedure.

Due to the tube insert, the flow passage in tubes is blocked. Consequently, the streamwise velocity development would be different from those without inserts. This also results in a fully-developed turbulent velocity profile that develops earlier than the usual bare tube does as the hydraulic diameter D decreases. This can be explained by the fact that when the configuration having a smaller D like tubes with inserts, the fully-developed condition would be reached sooner than those with a higher D, like tubes without inserts, due to a quick momentum exchange happening in tubes with inserts.

4.2. Azimuthal velocity profile and turbulent intensity

It is known that the flow through a tube with strip insert is characterized by a secondary flow field caused by unbalanced shear forces. Secondary flow produces a transport of fluid over the cross-section of the tube, causing the axial velocity profile to shift toward the tube wall. The fluid is forced outward, causing higher pressure to balance the momentum caused by secondary flow. For instance, in Fig. 4(e), at $x/d = 26$, the deviation in velocity is about 0.18 between $r^+ = 0.44$ and 0.472.

The symmetry of the present velocity profile in tubes with five different inserts was examined for different azimuthal angles (i.e. angular positions) at the same Reynolds number ($Re = 19\,500$) at $x = 270$ cm as shown in Fig. 9. The symmetry holds as one would expect for a bare tube (i.e. without insert) when compared with the present streamwise velocity (u) for four different azimuthal velocity profiles ($\theta = 0°, 45°, 90°$ and 135°). The situation is preserved for Fig. 9(b)–(d) until AR = 5 for both LS and CS inserts as shown in Fig. 9(e) and (f), respectively. The maximum dimensionless velocity $u_{max}/u_0 (\cong 1.15)$ at $r^+ = 0.62$ was found in Fig. 9(c) for AR = 4 with a LS insert. The maximum velocity for all the cases studied coincides with the geometrical centerline (shown in Fig. 9) of the flow passage (between the tube wall and insert). Actually, due to the symmetry nature of the present system and boundary condition, the symmetry of the velocity profiles would still stand. At AR = 5, for both LS and CS inserts, the asymmetry

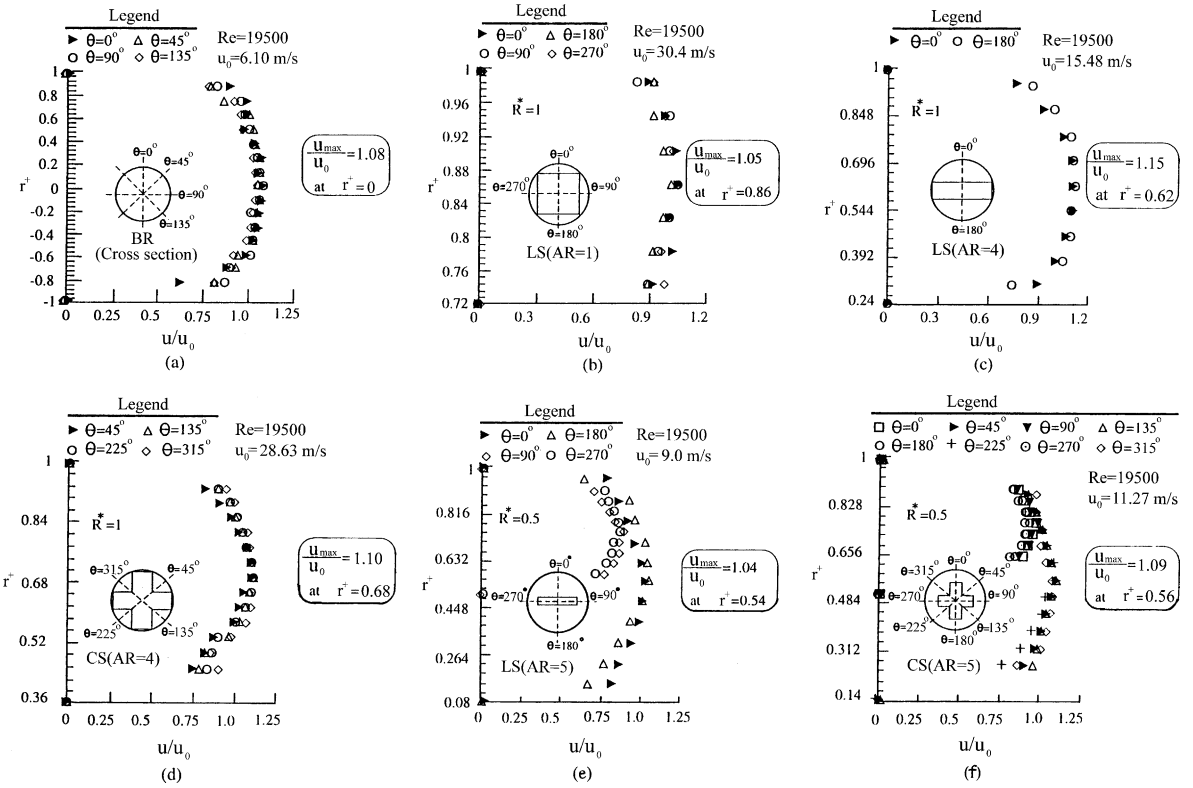

Fig. 9. Mean velocity distributions at different angular measuring positions in the fully developed region (at $x = 270$ cm) for tube with or without inserts.

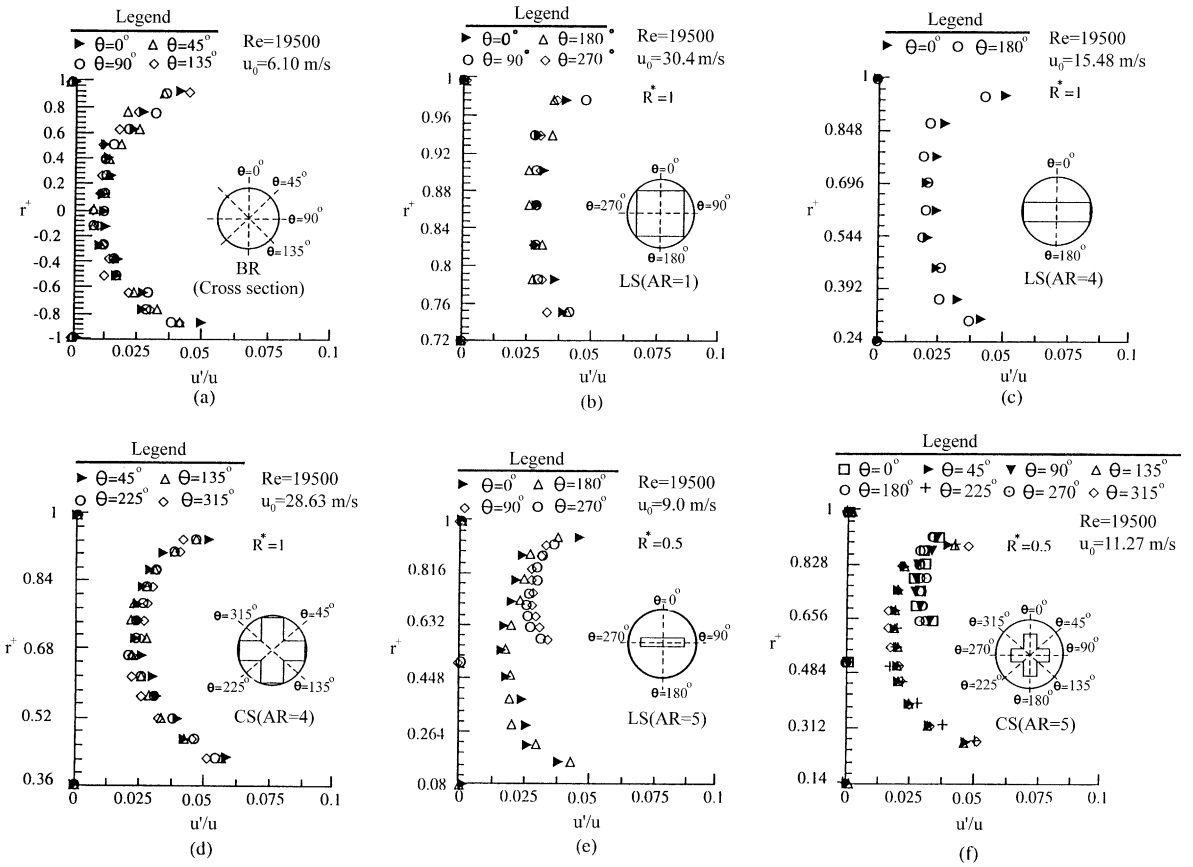

Fig. 10. Turbulent intensity distributions at different angular measuring positions in the fully developed region ($x = 270$ cm) for tube with or without inserts.

in the axial velocity profiles may be caused by the measured errors at $0.117 \leqslant r^+ \leqslant 0.264$ (Fig. 9e) and $0.243 \leqslant r^+ \leqslant 0.312$ (Fig. 9f) for $\theta = 0°$ and 180° (Fig. 9e) and $\theta = 225°$ and 315° (Fig. 9f). By comparing profiles in Fig. 9, one can see that the general profile shapes are approximately the same at this flow rate ($Re = 19\,500$) except for the cases of LS (AR = 5, $R^* = 0.5$) and CS (AR = 5, $R^* = 0.5$). The same situation exists for the corresponding figure for turbulent intensity (see Fig. 10). Furthermore, the axial velocity distribution indicates that, due to the adiabatic rectangular plate LS (AR = 5)/or crossed-strip plate CS (AR = 5) concentrically in the present tube, two sets of spiraling vortices (two/or four vortices) on the plane perpendicular to the direction of flow reported in Hsieh and Wen [8] which are symmetrical about a vertical midplane were formed as evident from Fig. 9(e) and (f). This is because the fluid is uniformly circumferentially heated by friction at the tube wall with the assumption of a negligible heating friction at the surface of the inserts, the fluid near the outer wall is warmer than the bulk fluid in the core. As a consequence, two upward currents flow along half of the side walls and, by continuity, the heavier fluid near the center of the tube flows downwards.

The velocity fluctuations (turbulent intensity) at different angular positions in terms of local mean velocity as u'/u for tubes with/without inserts are shown in Fig. 10. As seen from this figure, u'/u generally attains its maximum near the wall and its minimum near the center. Moreover, the axial turbulent intensity data are in good agreement with previous findings [9] for bare tube shown in Fig. 10(a). It seems there is no significant change in magnitude (<6%) in tubes with and without inserts. However, with inserts, the turbulent intensity distribution becomes more uniform especially for the case of LS (AR = 1) as compared to tubes without inserts due to a possible higher mixing caused by the present inserts. The relatively uniform distribution compared to that of bare tubes in axial turbulent intensity for the tubes with inserts suggests that viscous effects were negligible in this region. This can also explain the difference between the mean velocity distributions over the tube with inserts

and for bare tube as shown in Fig. 9. Based on the velocity and turbulent intensity measurements, it is found that shear between the fluid and the fluid in the core would increase the pressure drop and with insert it provides an additional longitudinal (LS; due to continuously interrupting the boundary layer)/cross (CS; due to continuously generating the secondary flow) mechanism for mixing.

4.3. Law of the wall for ($y^+ \geqslant 30$) the velocity profile

Correlation of the law of the wall was based on the velocity distribution measurement in the fully developed region (at $x = 270$ cm) for different Re. As is known, for the portion of the flow near the wall, ($y^+ \geqslant 30$) the velocity distribution is given by

$$u^+ = 2.5 \ln\left(\frac{y^+}{\eta}\right) + 5.5 \tag{2}$$

where $u^+ (= u/u^*)$ is the mean velocity normalized by the friction velocity, y^+ is the dimensionless vertical distance from the reference wall defined as yu^*/v. The typical velocity distribution of Eq. (2) is shown in Fig. 11. It is found that the discrepancy shows in Fig. 11 between the bare tube and the tubes with inserts. The results of bare tubes were obtained from the present study were compared to the results of Carr et al. [9]. As can be seen, the result for bare tubes is nearly the same as that of Carr et al. [9]. Overall, good agreement was observed, thereby confirming the reliability of the technique for the measurement of average velocity profile. In Eq. (2), $\eta(\geqslant 1)$ is the insert-affected coefficient that determines the shift in the smooth-wall logarithmic velocity profile caused by the present inserts and is 1 for a smooth wall. It is noted that, LS(AR = 5) has the biggest shift among the tubes with inserts.

4.4. Pressure drop and friction factor

Pressure distribution measurements were obtained for determining fully developed friction factors, so that the fluid flow inlet conditions were not an issue. The pressure drop was measured successively from the upstream to the downstream end for each of the six tubes under study at different Reynolds numbers. Eight (bare tube) and thirteen (with inserts) positions were measured for the present study. For five different Reynolds numbers, pressure gradient (Δp) along the test section was

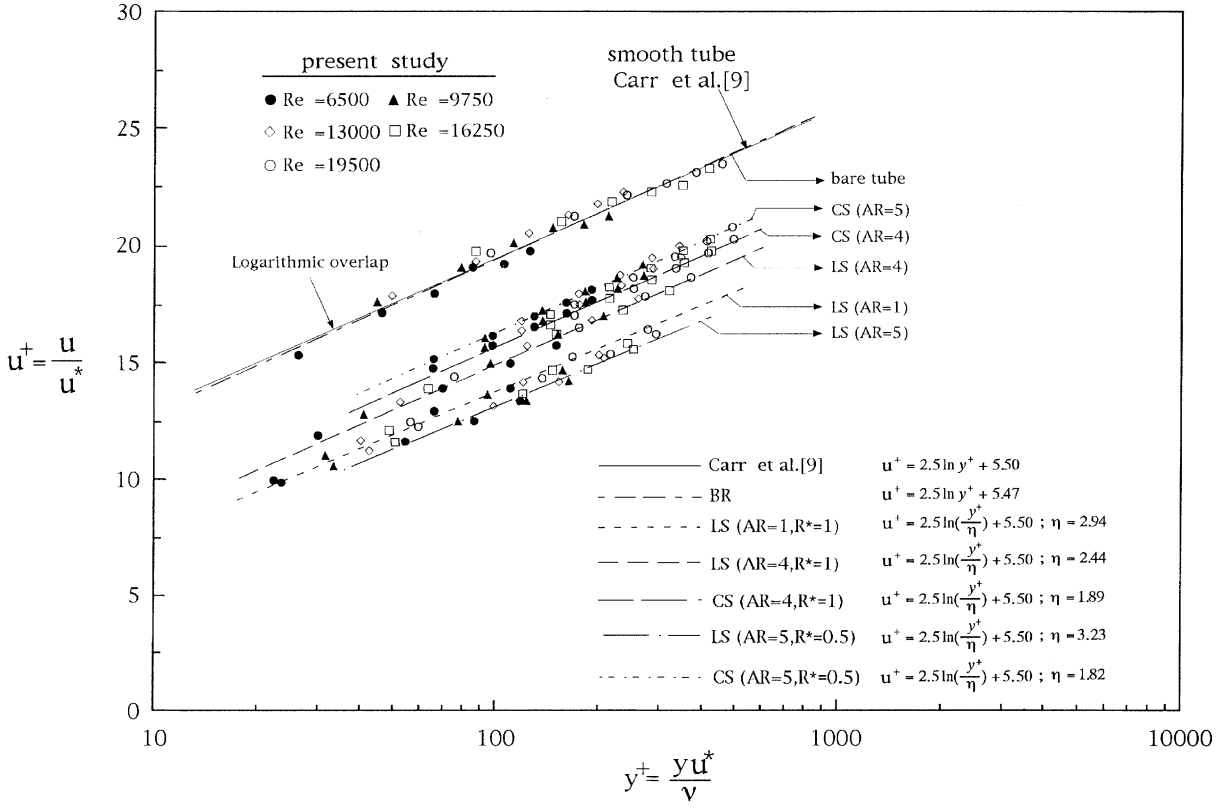

Fig. 11. Law of the wall for velocity distribution in the fully developed region.

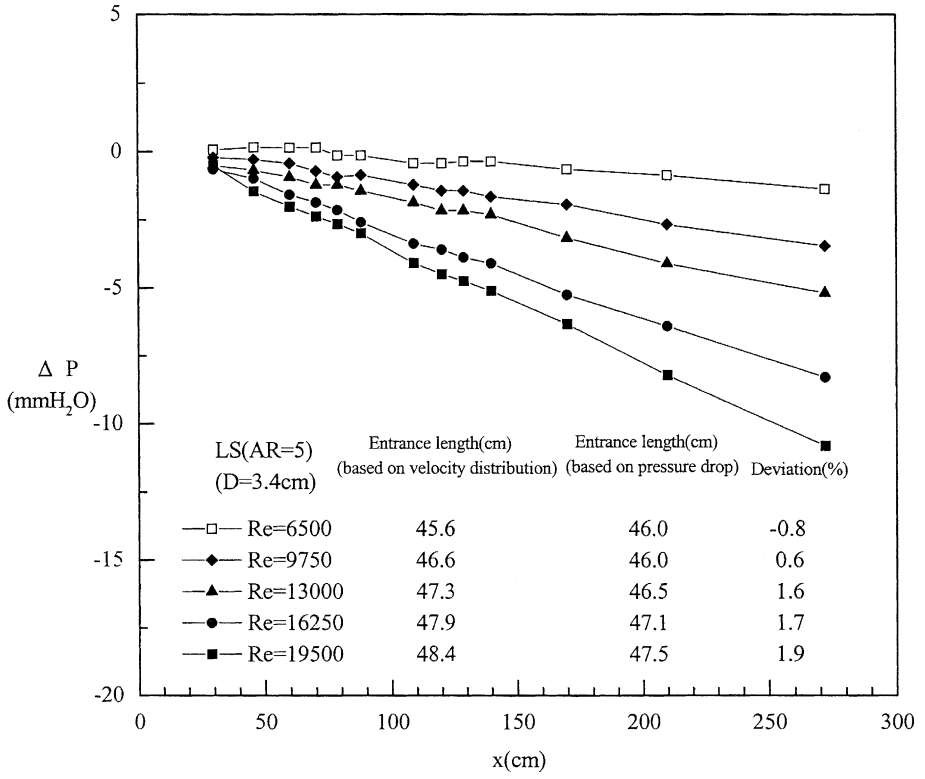

Fig. 12. Pressure drop distribution along downstream distance for the tubes with LS insert (AR = 1).

constant and the flow was therefore, fully developed. The entrance length based on pressure gradient can also be found and are in good agreement with those obtained from velocity measurement within ±5%. Typical results are shown in Fig. 12 for tubes with LS inserts (AR = 1). Generally, Δp increases as Re increases. The bare tube has the smallest Δp drop while the tube with LS insert and AR = 1 has the largest. The geometry of the strip-type inserts appears to be better suited to generate high momentum exchange (higher average velocity) than to induce an effective mixing motion (secondary flow) in the core of the fluid caused by crossed-type inserts which create more opportunities for boundary layer disturbances, and this could explain the high increase in pressure drop.

The isothermal friction factor f (including entrance effect) is calculated based on the Darcy formula and D (hydraulic diameter) which is correlated in terms of relevant parameters of Re, D/ℓ, and AR (aspect ratio) through dimensional analysis within ±9% to the original data and plotted in Fig. 13 for six tubes studied herein. The results for bare tubes were compared with those of Blasius [6] and McAdams [10]. The agreements seem good within ±8%. The correlation showed that the Reynolds number dependency for the friction factor is the same with and without inserts. An increase in AR (i.e., with a thinner insert) results in a lower f due to a smaller blockage effect. Moreover, the effect due to insert is considerable with a friction factor increase as an increase of the insert length. For the same Reynolds number the friction factor of the air flowing in a tube with a strip insert is higher than that for a bare tube. Upon further inspection of Fig. 13, because the blockage effect (with a thicker insert) becomes less evident compared with the other factors (e.g. disturbances in main core flow,..., etc.) for crossed-strip inserts, the friction factor increases as AR increases; e.g. comparing CS (AR = 4, $R^* = 1$) and CS (AR = 5, $R^* = 0.5$) at the same Re. It was also found that the blockage effect seems strongly dependent on the thickness of the insert.

Overall, the present increase in the flow friction factor is probably due to the following effects:

1. the increase of surface area;
2. the increase of the disturbance in the main core flow;
3. the increase of the disturbance in the turbulent boundary layer;
4. the blockage effect mainly due to the thickness of the insert.

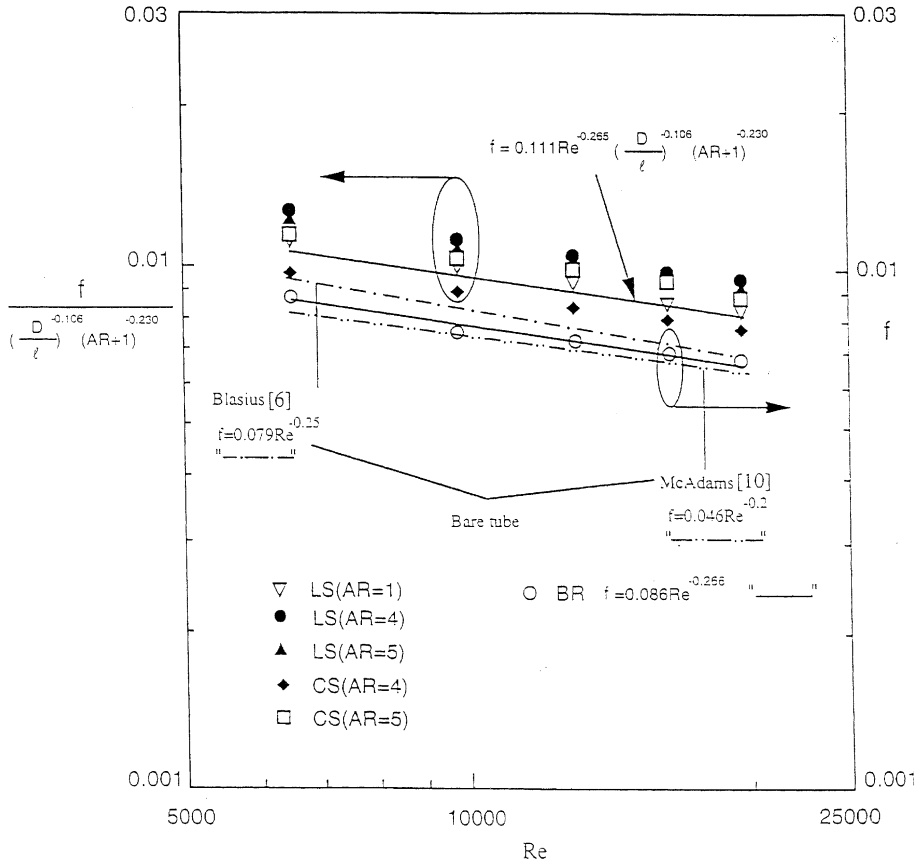

Fig. 13. A correlation fricion factor for five inserted tubes and comparison of friction factor correlations for bare tube.

5. Conclusion

The present experimental study of turbulent flow through a tube with strip type inserts has made it possible to examine for the first time the simultaneous effect of the parameters AR, R^* and Re. The effects on flow pattern and friction factor are presented. Correlations were developed for friction factors by using measuring data and compared with those existing data for bare tubes.

The following specific conclusions were drawn:

1. The hydrodynamic entry length with a tube insert was found to be shorter than that of a bare tube.
2. The azimuthal velocity profile and turbulent intensity show that symmetry in the angular profile exists for all the cases under study.
3. Mean velocity for law of the wall was developed for all the cases studied.
4. Friction factor increases for tubes with inserts as compared to bare tube values were typically between 1.1 and 1.5 for $6500 < Re < 19\,500$.

References

[1] S. Garimella, R.N. Christensen, Heat transfer and pressure drop characteristics of spirally fluted annuli: Part I—Hydrodynamics, ASME J. Heat Transfer 117 (1995) 54–60.
[2] A.E. Bergles, Augmentation of forced-convection heat transfer, in: S. Kakac, D.B. Spalding (Eds.), Turbulent Forced Convection in Channels and Bundles, Hemisphere Publishing Co, Washington, DC, 1973, pp. 883–909.
[3] F.F. Megerlin, R.W. Murphy, A.E. Bergles, Augmentation of heat transfer in tubes by use of mesh and brush inserts, ASME J. Heat Transfer 96 (1974) 145–151.
[4] S. Maezawa, G.S.H. Lock, Paper presented at Sixth Int. Heat Transfer Conference, Toronto, 1978.
[5] R.M. Manglik, A.E. Bergles, Heat Transfer and pressure drop correlations for twisted-tape inserts in isothermal tubes: Part II—Transition and turbulent flows, ASME J. Heat Transfer 115 (1993) 892–896.
[6] H. Blasius, Das Ähnlichkeitsgesetz bei Reibungsvorgängen in Flus-sigkeiten, Forschg. Arb. Ing. -Wes. 131 Berlin, 1913.
[7] R.J. Moffat, Describing the uncertainties in experimental results, Exp. Thermal Fluid Sci. 1 (1988) 3–17.
[8] S.-S. Hsieh, M.-Y. Wen, Developing three-dimensional laminar mixed convection in a circular tube inserted with

longitudinal strips, Int. J. Heat Mass Transfer 39 (1996) 299–310.
[9] A.D. Carr, M.A. Connor, H.O. Buhr, Velocity, temperature, and turbulence measurements in air for pipe flow with combined free and forced convection, ASME J. Heat Transfer 95 (1973) 445–452.
[10] W.H. McAdams, Heat Transmission, third ed., McGraw-Hill, New York, 1954.